Journal of
Water & Climate Change

IWA PUBLISHING

Journal of Water and Climate Change Vol 13 No 2, 557 doi: 10.2166/wcc.2021.282

Enhanced index for water body delineation and area calculation using Google Earth Engine: a case study of the Manchar Lake

Muhammad Ali Ismail [a,*], Maria Waqas [a], Amjad Ali [b], Mirza Muhammad Muzzamil [a], Uzair Abid[a] and Talha Zia[a]

[a] National Center in Big Data and Cloud Computing, Department of Computer and Information Systems Engineering (CISE), NED University of Engineering and Technology, Karachi 75270, Pakistan
[b] Centre for Advanced Studies in Pure and Applied Mathematics (CASPAM), Bahauddin Zakariya University, Multan 60800, Pakistan
*Corresponding author. E-mail: maismail@neduet.edu.pk

MAI, 0000-0003-0760-7051; MW, 0000-0002-8054-5128; AA, 0000-0003-1994-846X; MMM, 0000-0001-5258-8959

ABSTRACT

The sustainability of the hydrological and ecological ecosystems of any region requires continuous monitoring of the water bodies. Recent advancements in satellite-based remote optical sensors, big data analysis and cloud computing have given new dimensions to the field of water body studies including their detection as well as analysis. The present study extends the existing methods to assess the contemporary surface water detection and monitoring techniques via remote sensing. The proposed technique implies an improved hybrid approach for the purpose along with the calculation of the boundary areas. The study has been carried out on the Manchar Lake, the largest natural freshwater lake in Pakistan as well as in South Asia. The proposed hybrid water index along with the different existing water body detection indices and spectral bands have been worked out on the satellite images retrieved from the Google Earth Engine to detect and analyze the area/flow changes in the water body. Based on the 7 years of data, the proposed algorithm calculates the water body area more precisely. With limited availability of metadata about the study area, the results have been validated both qualitatively through national-met data and statistically. These results help to better preserve and improve the quality of the water resource.

Key words: Google Earth Engine (GEE), Landsat 8, Manchar Lake, Normal Difference Built-Up Index (NDBI), Normalized Difference Water Index (NDWI), water body detection

HIGHLIGHTS

- The present work studies Manchar Lake, the largest water body located in the Sindh province of Pakistan.
- The present work proposes a new water index, WIBI, for delineation area calculation of the water bodies.
- This is the first limnological study to observe and display annual area variation trends for the lake.
- Study results can be used to better preserve and improve the quality of the water resources.

GRAPHICAL ABSTRACT

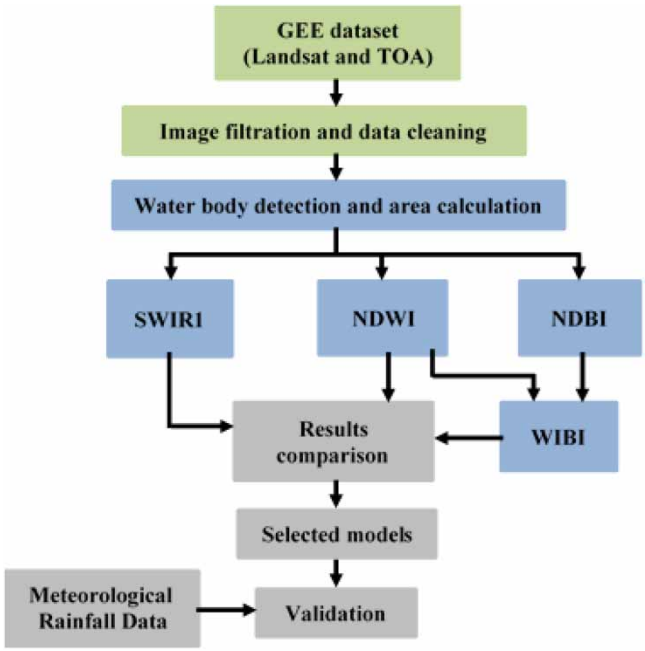

INTRODUCTION

Water is one of the key sources of life on Earth and is constantly changing. Waves batter the coast causing erosion, river banks are transformed under the flow of water, glaciers melt, resulting in new lakes and wetlands, reservoirs and harbors are constructed and much more. The accurate estimation of these changes of surface water is crucial for better understanding and management of the natural and anthropogenic processes causing them. For decades, satellites have been used to accumulate large amounts of related information, resulting in multi-petabyte archives of images collected. However, during the last decade, due to recent developments in cloud computing and big data analysis, researchers were able to transform these massive amounts of data into valuable knowledge. The main limitations that prevented the analysis of these large archives of satellite data were their commercial nature. A major change that has enabled the exploration of surface water at high spatial and temporal resolutions was the opening of access to the Landsat mission data by the National Aeronautics and Space Administration (NASA) in 2009. However, it took five more years to ensure that the first global-scale research results would be produced where these datasets could be explored to their full extent (Hansen *et al.* 2013). Besides, in recent years, the number of satellites along with their technical characteristics has significantly increased, resulting in better spatial, temporal, spectral and radiometric resolutions. This rise of the satellite industry presents new scientific challenges, demanding more efficient and robust methods to process massive amounts of data. With the technological and methodological developments, the focus of the surface water analysis shifts towards planetary-scale analysis, enabling the development of a more complete understanding of the Earth's natural and anthropogenic processes. Until recently, such planetary-scale monitoring and long-term estimates of land-use changes with high spatial resolution were not feasible (Hansen *et al.* 2013; Pekel *et al.* 2016).

As the amount of data available from the satellites is enormous, its processing and analysis requires HPC. Here, cloud computing comes to the rescue by providing platforms for large satellite data analysis. One such leading resource is the Google Earth Engine (GEE) (Gorelick *et al.* 2017), which by providing access to a variety of satellite datasets along with computation power to process and analyze them, is rapidly removing barriers from using planetary-scale data. The initiative to provide free access to supercomputer power for non-profit organizations and researchers was mentioned in 2009 for the first time, followed by the official release of the platform in 2012. Since then, it has resulted in numerous academic achievements, which have helped to analyze and better understand the changes of Earth's surface that have happened in the last few decades (Malthus & Dekker 1995; Hansen *et al.* 2013; Pekel *et al.* 2016). The GEE provides a wide range of dataset collections

encompassing several years, covering geographical, climatic and terranean aspects of the Earth's surface. These data have been successfully used in the determination of environmental changes and societal impacts on various landforms on Earth (Gorelick *et al.* 2017). One specific topic of interest in this domain is the monitoring of changing dynamics of water bodies on Earth due to natural and anthropogenic processes (Sakamoto *et al.* 2007; Schaffer-Smith *et al.* 2017). High-tech, state-of-the-art Operational Land Imager (OLI) optical sensor of Landsat 8 satellite has improved spatial resolutions to 30 m with a 15 m resolution panchromatic band. It is very efficient in detecting surface water bodies of almost any kind. Other popular sensors with even better spatial resolution include IKONOS, QuickBird and SPOT-5, which can provide images with meter and sub-meter spatial resolutions which has made the detection of smaller water bodies possible now (Huang *et al.* 2018).

RELATED WORK

Many researchers have utilized satellite data for delineation of water bodies via spectral indices. Among some earlier works on normalized indices, researchers used unique derivative analyses on high spectral resolution subsurface reflectance and similar data to obtain high spectral resolution reflectance to be used as the basis for indices for the detection of inland water bodies (Malthus & Dekker 1995). Using the green and near-infrared (NIR) spectral bands of Thematic Mapper (TM) sensor of Landsats 4 and 5, the Normalized Difference Water Index (NDWI) was then introduced to define and enhance the features of open water bodies satellite imagery while distinguishing from soil and terrestrial vegetation features (McFeeters 1996). A modification to the NDWI was proposed in Xu (2006), calling it the Modified Normalized Difference Water Index (MNDWI) which uses Middle Infrared instead of NIR of Landsat TM. The MNDWI helped reduce and even remove land noise to extract information on a water body from the study area. Hui *et al.* (2008) used both the NDWI and the MNDWI to study the feasibility of using multi-temporal Landsat images for assessing the spatial–temporal change in water bodies including water inundation of marshlands. Wu *et al.* (2008) analyzed the spectrum characteristic of the water body and several other main surface features of water having characteristics in TM imagery to find that a water body could be easily separated from all other surface complements only by assisting a suitable threshold value using the spectrum difference law. Ji *et al.* (2009) suggested methods to evaluate appropriate thresholds for identifying the water features clearly. They simulated various satellite sensors and calculated NDWI for each case. Sun *et al.* (2012) compared three existing methods of delineating open water features to suggest an improvement for fast extraction of water features in remotely sensed imagery. Li *et al.* (2013) investigated the best performing NDWI model out of 11 models of the Advanced Land Imager data in land surface water map. El-Asmar *et al.* (2013) used the water indices approach and employed a set of six satellite images acquired between 1973 and 2011 for surface area change due to the severe anthropogenic activities of local water bodies using the NDWI and the MNDWI. A new Automated Water Extraction Index (AWEI) was introduced by Feyisa *et al.* (2014) that improved the classification accuracy in areas that include shadow and dark surfaces which are often misclassified by other classification methods. Another evaluation of the NDWI was reported in Rokni *et al.* (2014). Song *et al.* (2014) evaluated uncertainties or accuracy of detecting lake area and water-level changes from multi-source satellite data.

Later researchers employed some non-normalized indices, machine-learning and other modern computational techniques to derive better results when working with the water bodies. A combination method had been applied in Wu *et al.* (2008) for water body extraction using Enhanced Thematic Mapper (ETM+) data based on a spatial combination mask of the spectrum-photometric method index and the tasseled cap wetness index and removing other objects from the mask image using the maximum likelihood classifier. Huang *et al.* (2015) proposed a novel two-level machine-learning framework to identify the water types from urban high-resolution remote-sensing images by extracting water bodies at pixel level and later identifying water types at object level achieving satisfactory accuracies. In a study by Sarp & Ozcelik (2017), spatio-temporal changes were evaluated using the multi-temporal Landsat TM and ETM+ images using support vector machine (SVM) classification and spectral water indexing, including NDWI, MNDWI and AWEI. In Yang *et al.* (2017), the researchers evaluated the performance of a newly available multispectral instrument (MSI) imagery for mapping water bodies using the image sharpening approach using NDWI and MNDWI. The result showed accuracy in the method for extracting the water body including river branches and small water areas, with a higher precision compared to the other methods. Sun *et al.* (2017) proposed a novel method called low albedo fraction for urban surface water, showing marked improvement over NDWI, MNDWI and AWEI. Acharya *et al.* (2017) successfully experimented with a combination of NDWI, Water Ratio Index and Normalized Difference Vegetation Index (NDVI) to derive a new index very suitable for binary classification of surface water. Campos & Brito

(2018) evaluated the performance of three previously proposed NDWIs using a multi-temporal series of Landsat 5 TM and Landsat 7 ETM+ images to derive maps with seasonal and permanent water in arid and semi-arid regions. Another comparison study was reported in Acharya *et al.* (2018), where the authors compared NDVI, NDWI, MNDWI and AWEI. Jiang *et al.* (2018) proposed a multilayer perceptron neural network as a better alternative for identifying the water bodies than using the normalized indices or SVMs. Wang *et al.* (2018) worked on finding area variation of a water body using vegetation index, water index and the random forest machine-learning technique. Acharya *et al.* (2019) used six different machine-learning algorithms for the same purpose. Integration of LiDAR data and multi-temporal aerial imagery was used by Wu *et al.* (2019) not only for water body detection but also to analyze its hydrological dynamics. Pickens *et al.* (2020) identified challenges in monitoring area variations in a water body using medium quality temporal and spatial satellite data. Markert *et al.* (2020) proposed and compared two unsupervised thresholding surface water mapping algorithms based on the histograms obtained from GEE. Wagle *et al.* (2020) combines normalized water indices such as MNDWI, Normalized Difference Built-Up Index (NDBI) and NDVI data over a decade from GEE using the XGBoost classifier to study temporal water area variations. Li *et al.* (2021) proposed three novel indices, namely Contrast Difference Water Index, Shadow Difference Water Index and a combination of the two, by improving MNDWI.

Thus, there is a long and comprehensive history of employing satellite imagery data for a wide range of applications, ranging from delineation of water bodies to monitoring their area variations using different kind of indices, to the study of atmospheric and anthropogenic effects on water bodies. This paper presents an extended research work on delineation of a very prominent water body called Manchar Lake located in the Sindh province of Pakistan. Multispectral satellite imagery has been used to calculate the spectral indices that are then used to measure the surface area of the water body. Introducing a simple but novel index, WIBI for calculating the area of the lake and setting the procedure for monitoring it all year round is the main purpose of this study. This is the first limnological study to observe and display annual area variation trends for the lake under study, which can be used to generate area variation trends for the water body during different times of the year. The study results can further be used to better preserve and improve the quality of the water resource. For an agricultural country like Pakistan, the availability and quantity of water resources during different parts of the year is of key importance. The process can be repeated for other water bodies of the country too and is anticipated to affect the overall agricultural turnover positively.

STUDY AREA

Manchar Lake, known as the floating village of Pakistan, is the biggest freshwater lake in the country, lying 18 km west of Sehwan Sharif on the Indus Highway. Figure 1 shows the geographical location map of this lake with relevant parameters. It is also the largest lake in South Asia. For hundreds of years, this lake has been home to many fishermen living on wooden boathouses. Moreover, fisher folk, known as Mirbahar or Mohannas, have been living here for centuries and survived on the available fish stock in the lake. The vicinity and banks of the lake enjoy a rich archaeological history dating back to Harappan culture. The lake has irregular boundaries with areas seasonally changing, ranging between 228 and 250 km^2. The depth varies from 0.5 to 3.75 m.

The main water sources for this lake include the river Indus and Kirthar hill torrents. The lake also receives polluted and toxic drain waters containing industrial and agricultural wastes from Main Nara Valley, which is gradually depleting the fresh waters of the lake. The government has planned to divert the drain to the Arabian Sea via the Right Bank Outfall Drain (RBOD). Despite its increasing contamination, the lake occupies an important regional position in the surrounding arid area.

The lake serves as the main water source for numerous villages around the Dadu district of Sindh for irrigation as well as domestic use. The lake is the habitat for around 200 fish species, providing means of living to a large number of fishermen. It also provides a pleasant recreation place providing a tourism boost as well. Last but not least, it attracts migratory birds for breeding. Figure 2 shows some camera shots demonstrating the beauty of the lake.

Thus, the importance of this study is two-fold; methodologically, it introduces a new index, and limnologically, the lake is of prime importance in the province. This study has been conducted to observe area variations in the lake throughout the year and over years to display trends which can been utilized to analyze different factors like the amount of different types of chemicals and contaminations in the lake. These results can thus be used to better preserve and improve the quality of this water resource.

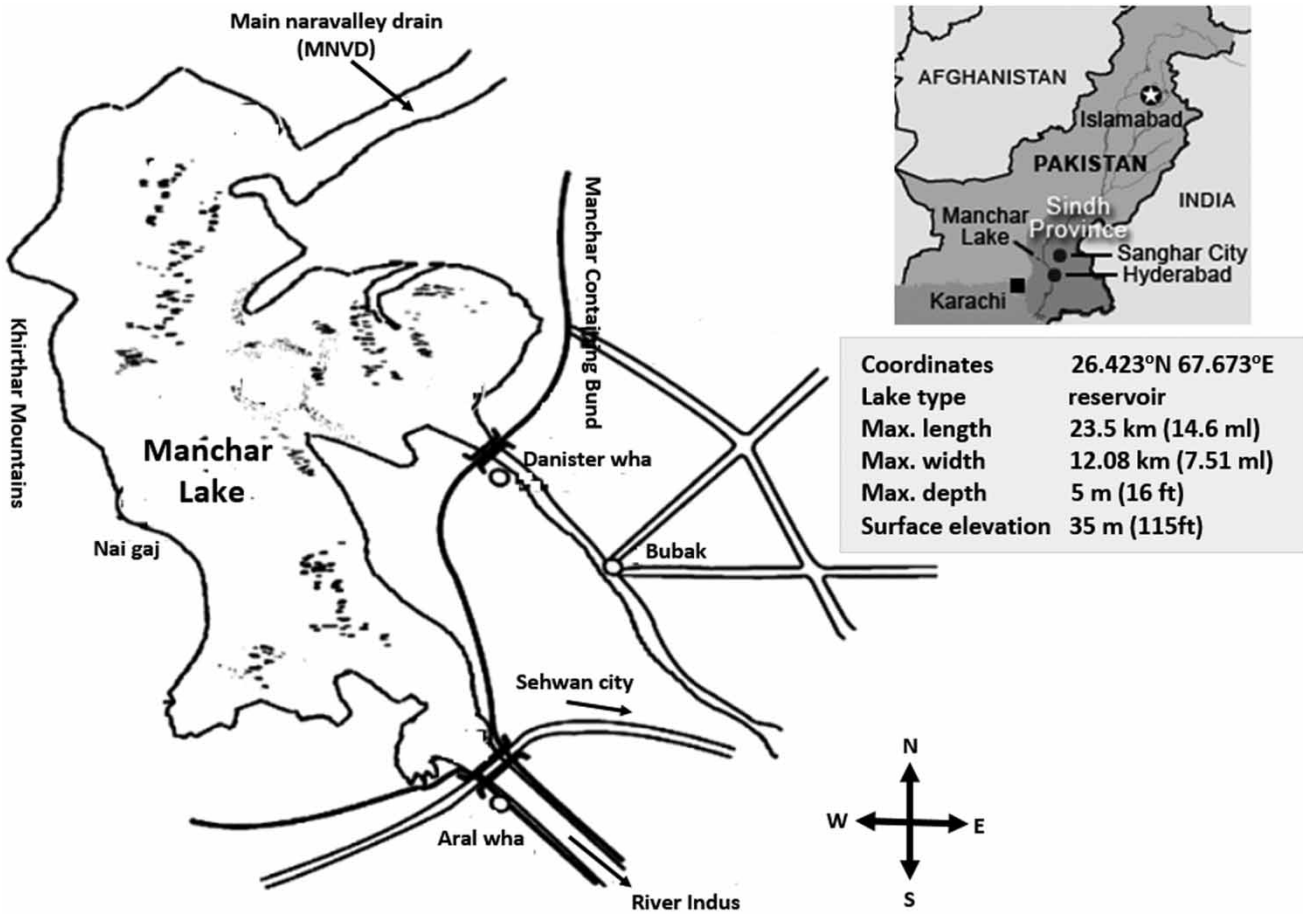

Figure 1 | Location map along with important characteristics of the Manchar Lake.

MATERIALS AND METHODS

Remote sensing satellite and dataset

The data used for this research were obtained from Landsat 8 satellite. Landsat 8 was launched on 11 February 2013, as a collaborative project between NASA and United States Geological Survey (USGS). Since then the satellite has been collecting multispectral images of the Earth's surface, available freely, on a global basis. The Landsat 8 satellite revolves around the Earth in 99 min. It has been placed at an altitude of 705 km (438 mi) with inclination of 98.2°. The satellite has a 16-day repeat cycle with an equatorial crossing time: 10:00 a.m. $\pm$15 min. This satellite acquires data on the Worldwide Reference System-2 (WRS-2) path/row system from Equator to extreme latitudes, with sidelap/swath varying from 7 to 85%, respectively. The scene size is 183 km$\times$170 km (106 mi$\times$114 mi). The state-of-the-art optical and thermal sensors boarded on this satellite include the OLI and the Thermal Infrared Sensor (TIS) (USGS.gov, Science for a changing world). OLI is known for its improved signal-to-noise ratio resulting from radiometric precision over a 12-bit dynamic range, enabling improved land cover condition and state characterization (USGS.gov, Science for a changing world). The TIRS sensor with a design life of 3 years collects image data for two thermal bands with a 100 m spatial resolution over a 190 km swath using two thermal infrared bands. The sensors of Landsat 8 support nine spectral bands. Nomenclature, wavelengths and resolutions of these bands are shown in Table 1.

The dataset used in this research comprises 154 images from Level 1 Landsat 8 Collection 1 calibrated top-of-atmosphere (TOA) reflectance, dated between 2013 and 2019 over the study area using the GEE platform. In selecting the dataset, special attention has been paid to images containing no clouds, fog and haze over the study area. Since NDWI performs better with reflectance images than digital number value images, TOA reflectance images have been utilized in this study. One spectral band, SWIR1, one normalized index, NDWI and one modified index have been employed and compared to detect the water

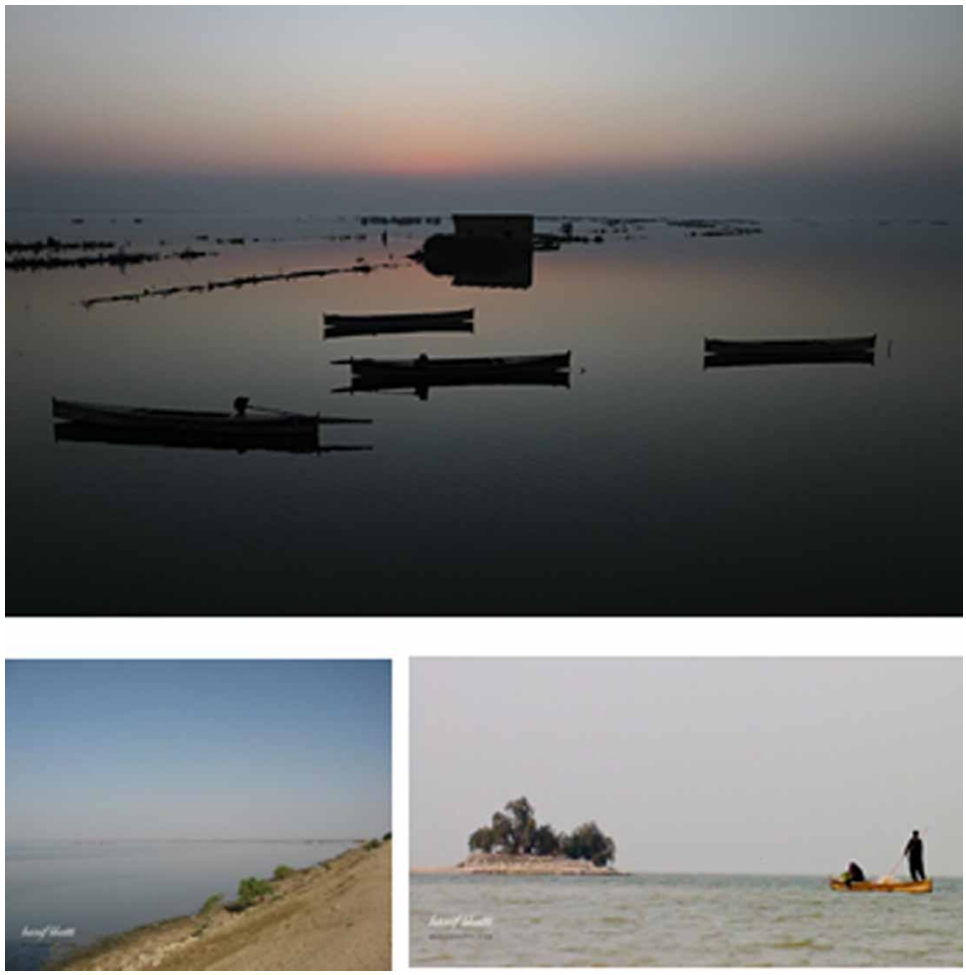

Figure 2 | Images of the Manchar Lake.

Table 1 | Landsat 8 OLI and TIRs (USGS.gov, science for a changing world)

Band	Resolution (m)	Wavelength (μm)
Band 1 – Coastal aerosol	30	0.43–0.45
Band 2 – Blue	30	0.45–0.51
Band 3 – Green	30	0.53–0.59
Band 4 – Red	30	0.64–0.67
Band 5 – NIR	30	0.85–0.88
Band 6 – SWIR 1	30	1.57–1.65
Band 7 – SWIR 2	30	2.11–2.29
Band 8 – Panchromatic	15	0.50–0.68
Band 9 – Cirrus	30	1.36–1.38
Band 10 – TIRS 1	100	10.6–11.19
Band 11 – TIRS 2	100	11.50–12.51

body in focus. The existing NDWI model used combines two bands, Green and NIR, and is considered the most effective index in the majority of scenarios. The modified index has been derived by subtracting NDWI from NDBI. The MNDWI model has been referred to as WIBI in the remainder of this paper. This band-related information along with the spectral

index equations and threshold values used in this study have been summarized in Table 2 and described further in the following text.

Of 154 images, obtained from the GEE dataset, 113 images were selected and 41 images were rejected due to the presence of clouds, haze and missing data over the study area. The data acquisition dates for all the selected 113 images are tabulated in Table 3. Each selected image is then subjected to the selected water body detection band SWIR1 and indices including NDWI

Table 2 | Spectral indices and bands along with their equations

NDBI	Band	Spectral index equation	Threshold values
SWIR1	6	–	0.1
NDWI	3 and 5	(Green − NIR)/(Green + NIR)	0.2
WIBI	–	NDWI − NDBI	0.3
NDBI	–	(SWIR − NIR)/(SWIR + NIR)	–

Table 3 | List of acquisition dates of Landsat-8 OLI images of Manchar Lake

Sr. No.	Date	Sr. No.	Date	Sr. No.	Date	Sr. No.	Date
1.	23-May-13	30.	01-Oct-14	59.	13-Apr-16	88.	28-Dec-17
2.	08-Jun-13	31.	17-Oct-14	60.	29-Apr-16	89.	13-Jan-18
3.	24-Jun-13	32.	02-Nov-14	61.	15-May-16	90.	29-Jan-18
4.	10-Jul-13	33.	18-Nov-14	62.	03-Aug-16	91.	02-Mar-18
5.	11-Aug-13	34.	04-Dec-14	63.	19-Aug-16	92.	18-Mar-18
6.	27-Aug-13	35.	05-Jan-15	64.	04-Sep-16	93.	03-Apr-18
7.	12-Sep-13	36.	21-Jan-15	65.	20-Sep-16	94.	19-Apr-18
8.	28-Sep-13	37.	06-Feb-15	66.	06-Oct-16	95.	05-May-18
9.	14-Oct-13	38.	10-Mar-15	67.	22-Oct-16	96.	21-May-18
10.	30-Oct-13	39.	11-Apr-15	68.	07-Nov-16	97.	06-Jun-18
11.	15-Nov-13	40.	13-May-15	69.	23-Nov-16	98.	22-Jun-18
12.	01-Dec-13	41.	29-May-15	70.	09-Dec-16	99.	09-Aug-18
13.	17-Dec-13	42.	14-Jun-15	71.	25-Dec-16	100.	25-Aug-18
14.	02-Jan-14	43.	16-Jul-15	72.	10-Jan-17	101.	10-Sep-18
15.	18-Jan-14	44.	01-Aug-15	73.	26-Jan-17	102.	26-Sep-18
16.	19-Feb-14	45.	17-Aug-15	74.	15-Mar-17	103.	12-Oct-18
17.	07-Mar-14	46.	02-Sep-15	75.	16-Apr-17	104.	28-Oct-18
18.	23-Mar-14	47.	18-Sep-15	76.	18-May-17	105.	15-Dec-18
19.	08-Apr-14	48.	04-Oct-15	77.	03-Jun-17	106.	16-Jan-19
20.	24-Apr-14	49.	20-Oct-15	78.	19-Jun-17	107.	05-Mar-19
21.	10-May-14	50.	05-Nov-15	79.	06-Aug-17	108.	22-Apr-19
22.	26-May-14	51.	21-Nov-15	80.	22-Aug-17	109.	24-May-19
23.	11-Jun-14	52.	07-Dec-15	81.	07-Sep-17	110.	09-Jun-19
24.	27-Jun-14	53.	23-Dec-15	82.	23-Sep-17	111.	25-Aug-19
25.	13-Jul-14	54.	08-Jan-16	83.	09-Oct-17	112.	29-Sep-19
26.	29-Jul-14	55.	09-Feb-16	84.	25-Oct-17	113.	15-Dec-19
27.	14-Aug-14	56.	25-Feb-16	85.	10-Nov-17		
28.	30-Aug-14	57.	12-Mar-16	86.	26-Nov-17		
29.	15-Sep-14	58.	28-Mar-16	87.	12-Dec-17		

and WIBI to detect the area of the studied lake. Some of the graphical results presented in this paper have been shown for three times of each year, winter, summer and right after monsoon. The main reason behind choosing 3 months/year was that the months right after the summer of the year are most affected by monsoon which obscure images completely due to cloud or haze. As mentioned above, such images have already been removed; their absence was making data inconsistent and to avoid this 3 months/year were carefully chosen. These 3 months are January as the winter month, May as the summer month and September as the post-monsoon month. For the first year which is 2017, January data are not available on GEE so only two times of the year have been shown. The observations and derived results are presented and discussed in the following section.

Methodology

The main objective of this research was to track variations in the area of Manchar Lake throughout the years. The text in this section summarizes the overall methodology used to gather and process data to achieve the objective. As stated earlier, the GEE hosts satellite imagery data and provides computational facilities over it through an easy web-based interface. This study accesses this facility through interactive JavaScript coding using the Earth Engine Code Editor. Landsat 8, TOA satellite images were used from GEE for a period of 7 years (2013–2019). The data were then filtered to remove the images having clouds, fog and haze factors. The shortlisted and cleaned dataset was then fed to the GEE processing module responsible for detecting the water body first. Afterwards, the area of the detected water body was calculated from the image through pixel counting. For detection of the water body, three existing bands/indices including SWIR1, NDWI and NDBI along with one new proposed index, WIBI, derived from NDWI and NDBI were considered. The results are then compared to select the best ones. Two criteria were used for the selection; first, the image quality, and second, by comparing the area values quantitatively with the available ones from the national authorities. The variations indicated by these selected results are also validated from the national meteorological data. This whole process is summarized in Figure 3.

Intuition behind WIBI

NDWI is a good index for delineation of water bodies with or without vegetation due to the usage of Green band, but may give overestimated results if buildup area is present. The NDBI employs SWIR band and is good for detecting buildup areas (Xu 2006; Gautam *et al.* 2015; Kshetri 2018). The intuitive understanding behind the proposed model is to combine the two bands to make the most of both features as required for the area under study. As stated earlier, the river is home for many fishermen living on floating boat houses, which keep changing places. However, more work needs to be done to validate

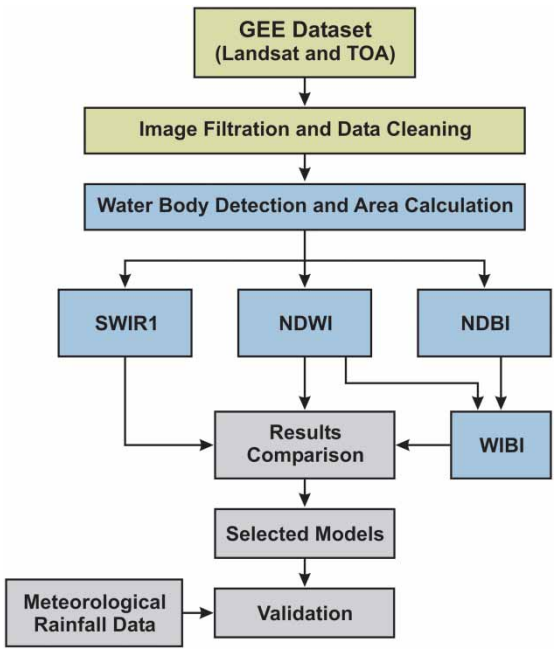

Figure 3 | Flow diagram representing the overall methodology adopted to collect, clean and process data used to detect the water body.

this intuitive line of reasoning by comparing the results with other indices using similar techniques. In this study, the validation is done through graphical comparisons and pixel-based area calculations.

WIBI threshold selection

The threshold selection process is illustrated in Figure 4. Figure 4(a) shows the acquired image from Landsat 8 TOA satellite. On this image, layer of WIBI was set to the difference of NDWI and NDBI to produce the binary image shown in Figure 4(b). The GEE provides an option to inspect individual pixels of the layer, so the image was inspected pixel by pixel to detect the water body in the region of interest and the corresponding pixel value of water is noted. This optimal threshold value came out to be 0.3. Figure 4(c) and (d), respectively, shows the images highlighting the thresholded area and otherwise. Figure 4(e) shows the corresponding histogram. A histogram was obtained for NDWI too with threshold set to the chosen value of 0.2. It can be seen from both histograms that WIBI gives lower frequency values at the selected threshold as compared to the NDWI.

WIBI calibration

As stated earlier, the Manchar Lake has irregular boundaries which keep on changing seasonally. Also, there is no official information available on the area of the lake; hence, we are considering the minimum area value for quantitative validation of the results obtained from GEE images. To validate the WIBI index itself, it was applied to find the area of a man-made water body with fixed boundaries. The water body selected for this purpose was an open-air swimming pool built in the Poruba district of the Czech Republic. The pool is one of the largest man-made water pools in Central Europe with a fixed surface area of 41,200 m^2 (Panoramas.cz n.d.). Table 4 shows the Landsat 8 image acquisition dates and the corresponding value of the area measured using the proposed index as well as the standard NDWI. Threshold (T) was set to 0.3 for WIBI. This is the same index that is used for the delineation of Manchar Lake. It can be seen that the calculated area values for the pool using WIBI are close to the actual area value as reported on official websites. Also, the area calculated over different dates is found to be consistent. Same delineation task was done using WIBI with the same index as set for the Manchar Lake, T=0.2, but it was observed that the results were not very consistent. Better results were obtained with T=0.08 for NDWI. This concluded that almost both indices, WIBI and NDWI, produced similar results, but NDWI is threshold sensitive, whereas WIBI is robust in this regard.

RESULTS AND DISCUSSION

The water body detection capabilities of NDWI, WIBI and SWIR1 derived from Landsat-8 OLI have been examined and compared in this research work. NDWI and WIBI data have been produced from 30 m resolution imagery. Results from each of the three datasets have been compared side by side and with the corresponding data produced by the national meteorological department to validate lake area variations.

Figure 5 shows satellite images of the Manchar Lake using different spectral bands and indices. Figure 5(a) is a SWIR 1 image. Short-wave infrared (SWIR) imaging uses light in the wavelength ranging between 0.9–1.7 and 0.7–2.5 μm and hence requires unique and optical and electronic components suiting this specific range. Figure 5(b) shows the NDWI images, which generates the best results for visible as well as infrared wavelengths. It easily distinguishes a water body from its surrounding built-up lands. The index for water bodies is >0.5, while that for vegetation and other built-up features is much smaller in the range of 0–0.2. NDBI is an index for the analysis of built-up area. As stated earlier, for bare-soil and built-up areas, SWIR has higher reflectance than NIR; while it is vice versa for green surfaces. Reflectance of water bodies is zero on infrared spectrum (Pakistan Meteorological Department n.d.).

Figure 5(c) shows the WIBI image. As stated earlier, for this research a modified index, WIBI, has been introduced which is computed as the difference between NDWI and NDBI. As can be seen from the four images of Figure 5, WIBI greatly enhances the water body detection, making it clearly visible. Along with the water body, it also classifies the soil and vegetation index in a good manner. The NDWI model used in this calculation is NDWI (Green, NIR) for its suitability for detecting green surfaces as compared to the other two NDWI versions. Here, values of water bodies are >0.2, while vegetation has much smaller values, which results in easy distinguishing of vegetation from water bodies. This technique proved a lot better than any NDWI versions and SWIR1 in separating the water pixels from the soil and vegetation.

For SWIR1, NDWI and WIBI, the chosen thresholds are 0.1, 0.2 and 0.3, respectively. The selection of thresholding method was based on the spectral characteristics of water and how it differentiates with other classes in terms of its spectral

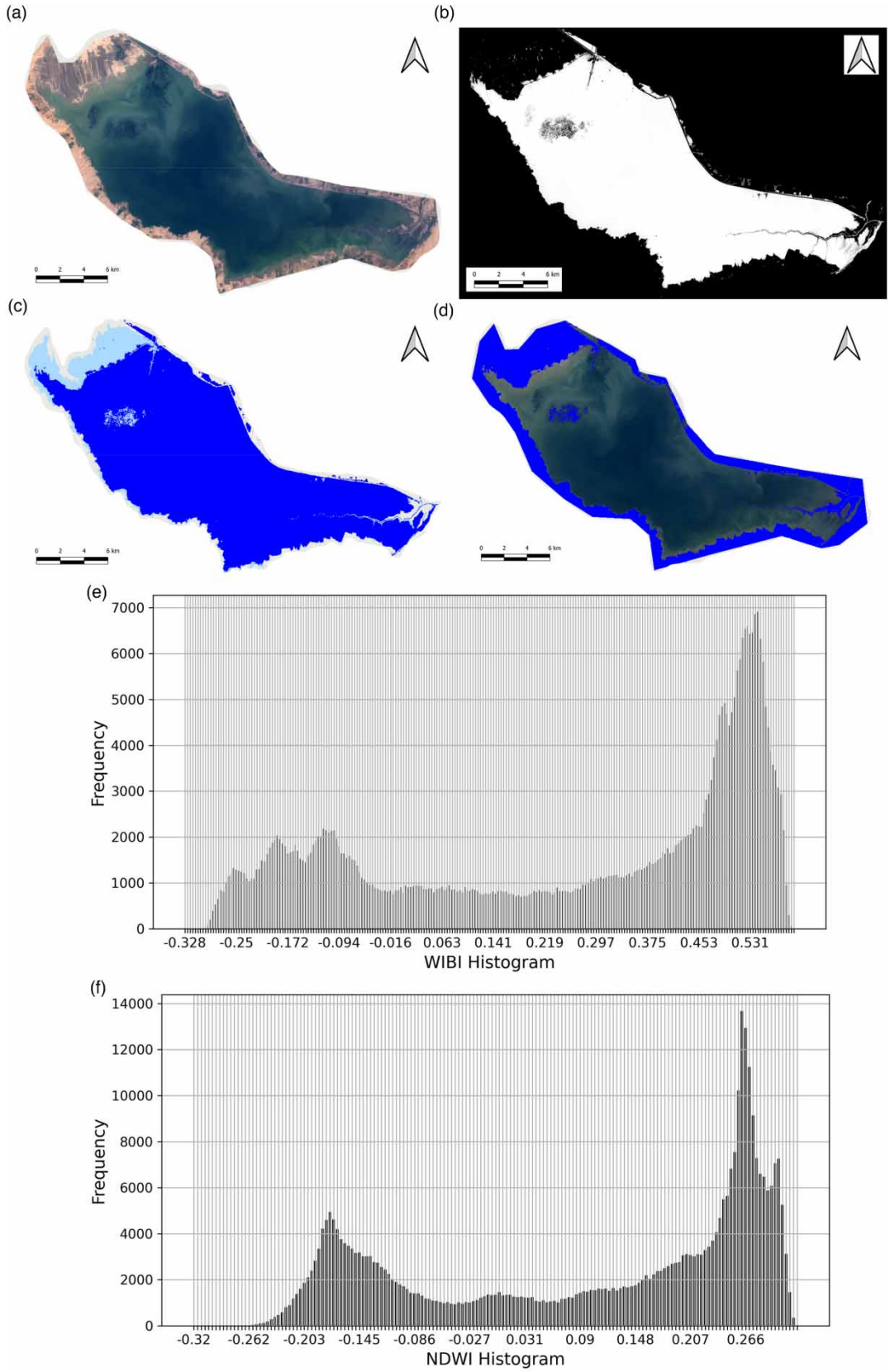

Figure 4 | Image thresholding process for an image using WIBI index. (a) Landsat 8 TOA image (acquisition date: December 15, 2018). (b) WIBI index binary image. (c) Image showing masking of water pixels after setting threshold to 0.3. (d) Image highlighting the regions where threshold is less than 0.3. (e) Histogram for WIBI. (f) Histogram for NDWI.

Table 4 | List of acquisition dates of Landsat-8 OLI images of the manmade pool

Sr. No.	Image acquisition date	Calculated pool area (m^2)		
		WIBI (T=0.3)	NDWI (T=0.2)	NDWI (T=0.08)
1.	13-Jul-13	40,670.34	0	40,670.34
2.	5-Jan-14	40,670.34	40,670.34	40,670.34
3.	13-May-14	40,670.34	40,670.34	40,670.34
4.	20-Oct-14	40,670.34	0	40,670.34
5.	1-Jun-15	40,670.34	13,581.49	40,098.71
6.	17-Jun-15	40,670.34	21,026.76	40,098.71
7.	5-Sep-15	40,670.34	9,244.87	40,670.34
8.	14-Feb-17	40,670.34	40,670.34	40,670.34
9.	5-Mar-18	40,670.34	40,670.34	40,670.34
10.	8-May-18	40,670.34	0	38,973.09
11.	14-Jul-19	40,670.34	40,670.34	40,670.34
12.	14-Jun-20	40,670.34	2,014.82	40,670.34
13.	4-Oct-20	40,670.34	40,670.34	40,670.34
14.	13-Mar-21	40,670.34	0	40,670.34
15.	29-Mar-21	40,670.34	0	40,670.34

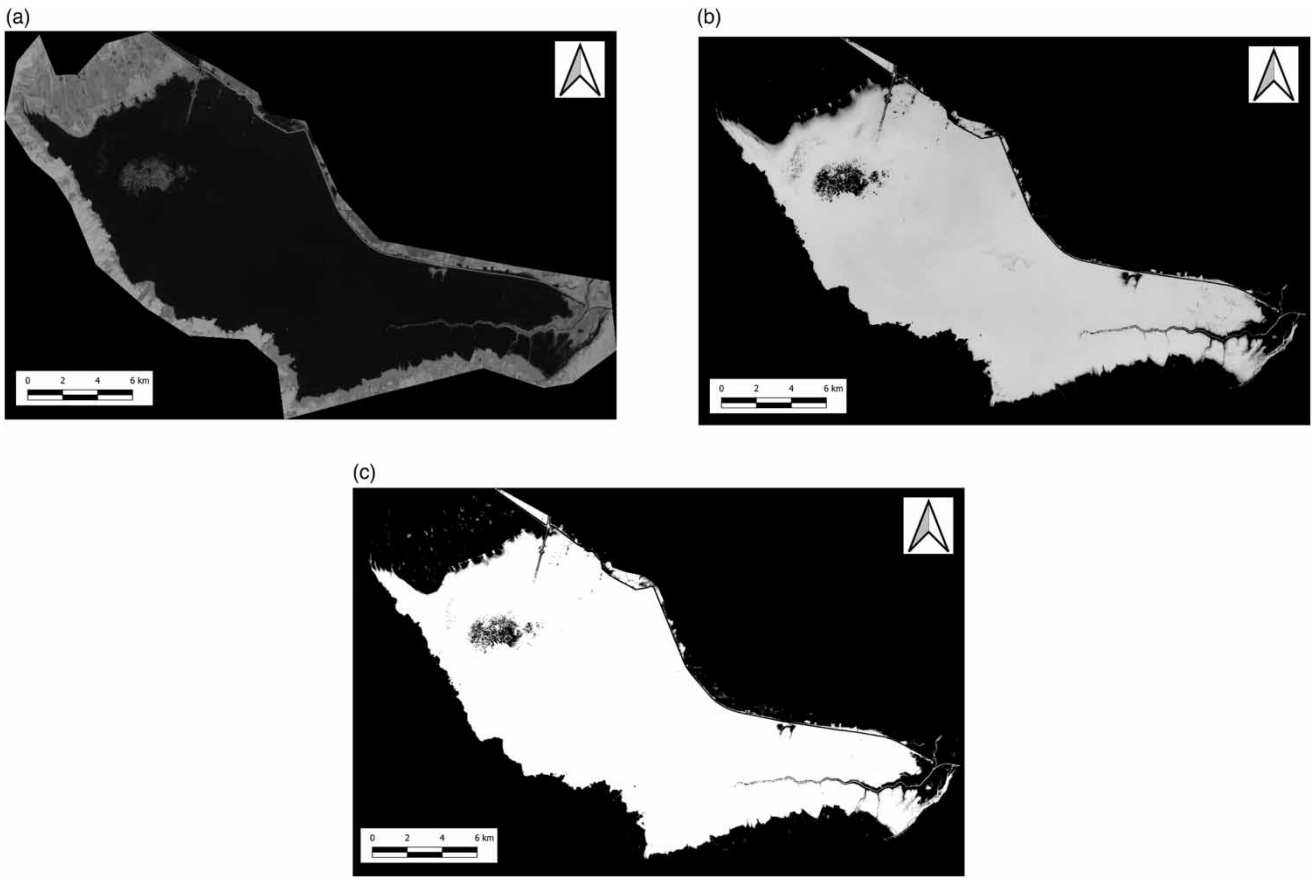

Figure 5 | Satellite (Landsat 8 TOA) images of Manchar Lake using spectral bands and indices (acquisition date: December 12, 2017). (a) SWIR1. (b) NDWI. (c) WIBI. Please refer to the online version of this paper to see this figure in color: http://dx.doi.org/10.2166/wcc.2021.282.

value. The range was selected carefully to suit a wide range of the selected imagery. These selected threshold values provided wrong area values for specific months when the haze was evident in the images. Reducing this threshold resulted in reduced delineation making water and non-water areas indistinct. The threshold values are indicated along with the images in Figure 6.

In Figure 6(a), the water body pixels are shown in black, while Figure 6(b) and (c) shows water body pixels in white color and the surrounding area is the distribution of non-water pixels. All these images have been taken on the same date to compare the water body pixels. As can be seen from these images, the three methods, namely SWIR1, NDWI and WIBI, proved efficient in detecting the area of the water body.

Yearly area variation trends using SWIR1, NDWI and WIBI

Table 5 shows the calculated area values in km^2 for the selected images of the Manchar Lake from the dataset of Landsat-8 TOA reflectance, at three different times of the year, January, May and September, for 7 consecutive years (2013–2019). These months are referred to as M1, M2 and M3, respectively, in the proceeding charts and figures. As stated earlier, data for January 2013 were not available in the GEE data stores.

Figure 7 plots the data given in Table 5, with lake area in km^2 on *y*-axis and month of a year on *x*-axis, displaying trends in area variation of the Manchar Lake during three different parts of the year for each year from 2013 to 2019. It can be seen that in almost all years, the lake area is on the higher side at the start of the year in winter (January, M1). The area drops to a very low value comparatively in summer (May, M2) due to heat and heavy consumption of water. The lake refills in the monsoon season so the area rises again after it (September, M3). One exception is the year 2014, where the area received extremely low rainfall during monsoons and remained extremely dry afterwards too; this has been verified by the met data which is discussed in a later section of this paper. Also, SWIR1, NDWI and WIBI all follow the same trend for each year.

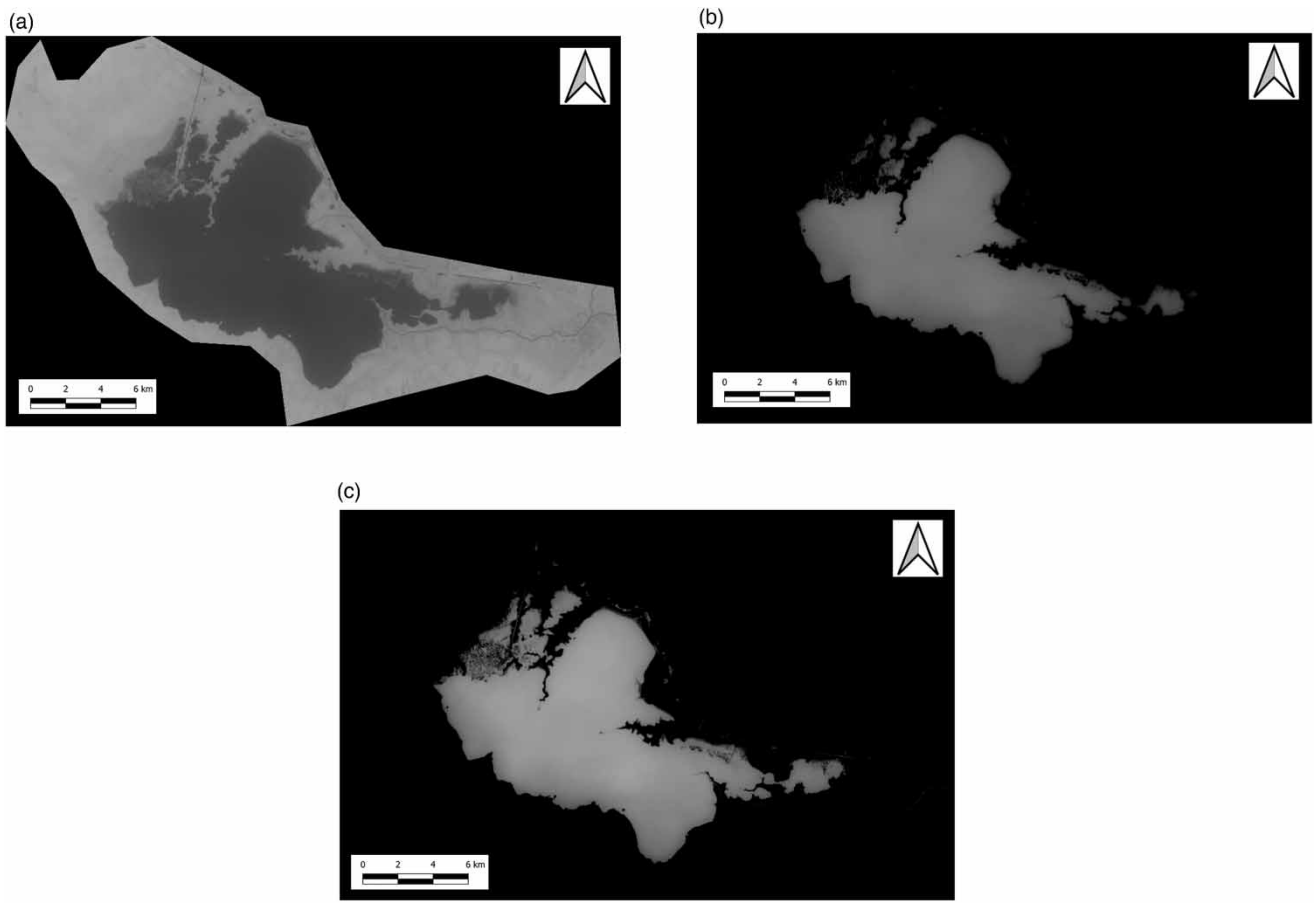

Figure 6 | Satellite images of Manchar Lake using spectral bands and indices with different threshold values (acquisition date: July 29, 2014). (a) SWIR1, threshold=0.1. (b) NDWI, threshold=0.2. (c) WIBI, threshold=0.3.

Table 5 | Tabulation of calculated area of Manchar Lake from satellite images, using the three methods, SWIR1, NDWI and WIBI, taken at three different times of the year (M1, M2 and M3) for seven consecutive years (2013–2019)

		Area (km^2)							
Year→		**2013**	**2014**	**2015**	**2016**	**2017**	**2018**	**2019**	**Average**
SWIR1	M1		197.20	221.43	208.89	243.18	222.24	222.24	212.82
	M2	180.83	183.50	189.38	148.46	220.70	226.34	226.34	
	M3	271.12	171.86	265.02	251.26	223.46	261.01	261.01	
NDWI	M1		185.28	210.80	192.69	234.62	213.74	213.74	196.64
	M2	142.60	164.62	146.54	123.49	198.70	212.16	212.16	
	M3	259.54	154.19	256.17	241.81	215.49	251.20	251.20	
WIBI	M1		199.64	225.49	215.19	246.18	225.01	225.01	216.10
	M2	183.14	187.82	193.19	157.13	222.72	230.15	230.15	
	M3	271.99	176.14	267.50	252.76	224.97	263.01	263.01	

M1, M2 and M3, respectively, refer to the three selected months of January, May and September.

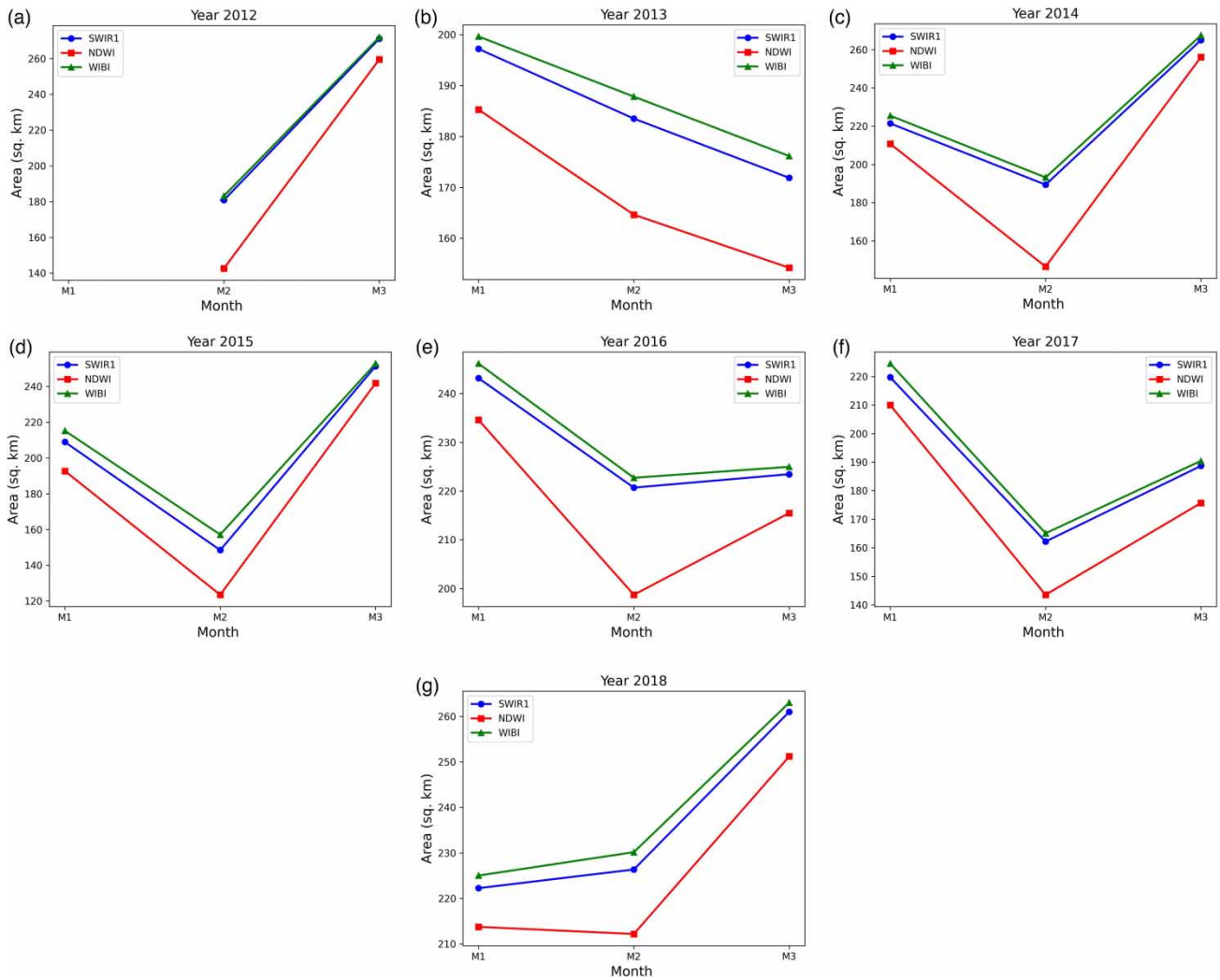

Figure 7 | Plots showing yearly area variation trends of Manchar Lake as obtained from satellite images, using the three methods, SWIR1, NDWI and WIBI, taken at three different times of years (M1, M2 and M3) for seven consecutive years (2013–2019). M1, M2 and M3, respectively, refer to the three selected months of January, May and September. (a) Year 2013. (b) Year 2014. (c) Year 2015. (d) Year 2016. (e) Year 2017. (f) Year 2018. (g) Year 2019.

Area variation trends in 7 years using SWIR1, NDWI and WIBI

Figure 8 consolidates and compares area variation trends of the Manchar Lake over the period of 7 years. The plots show area variation obtained through the three selected methods, SWIR1, NDWI and WIBI, respectively, from all 113 images. The plots take lake area in m^2 on *y*-axis, while *x*-axis represents the number for 113 dates on which the images have been acquired. The actual date can be inferred from Table 3. It can be observed from the plot that the lake area follows a general pattern with a few exceptions. The general trend is that the lake area is larger at the start of the year, shrinks to a lower value during summers, and then after monsoon goes back to its larger state by the end of the year. The unusual dips of Y5 (2017) and Y6 (2018) show very low area values, as water is consumed more quickly in these months as compared to winters, due to which the threshold values of lake area got higher than the actual threshold values.

Quantitative validation of results

The minimum area of the Manchar lake as reported by various resources is 228 km^2 and the maximum is 250 km^2 (Muzaffer *et al.* 2020). This gives an average of 239 km^2. In Pakistan, the relevant data are not readily available for public use and are seemingly not updated on a regular basis either. Therefore, the results of this study have been validated against the values as given above. The average values for lake area are calculated for each of the methods SWIR1, NDWI and WIBI and are also listed in Table 5. It can be seen that WIBI gives the closest average area value to the reported value. Recalling Figure 4, WIBI gave better visual results too. Hence, the proposed index seems promising and potentially useful for future work in this domain.

Qualitative validation of results through Pakistan Meteorological Department's data

Pakistan Monsoon 2013 Rainfall report as provided by the Climate Data Centre of Pakistan Meteorological Department during the month of July, unusually deficient monthly rainfall was observed almost all over the country but severe dryness was observed over the Sindh province. For the month of August, heaviest rainfall was recorded all over the country. The monthly rainfall in the Sindh province was largely above normal. The monsoon activity reduced significantly in the month of September in almost all the country. The recorded rainfall in the Sindh province was largely below normal.

For 2014, in the month of July, deficient rainfall was observed over Pakistan and below normal rainfall was recorded in Sindh. The severe rainfall deficit continued to persist in the month of August and below normal rainfall was recorded over Pakistan. Sindh received largely below normal rainfall. In September, rainfall increased all over Pakistan except Sindh which received less rainfall than the other provinces.

In the month of July 2015, almost the whole country received above normal rain, with Sindh being at the top where exceptionally high rainfall was recorded. In August, the situation was reversed for Sindh which faced high rainfall deficit, while the

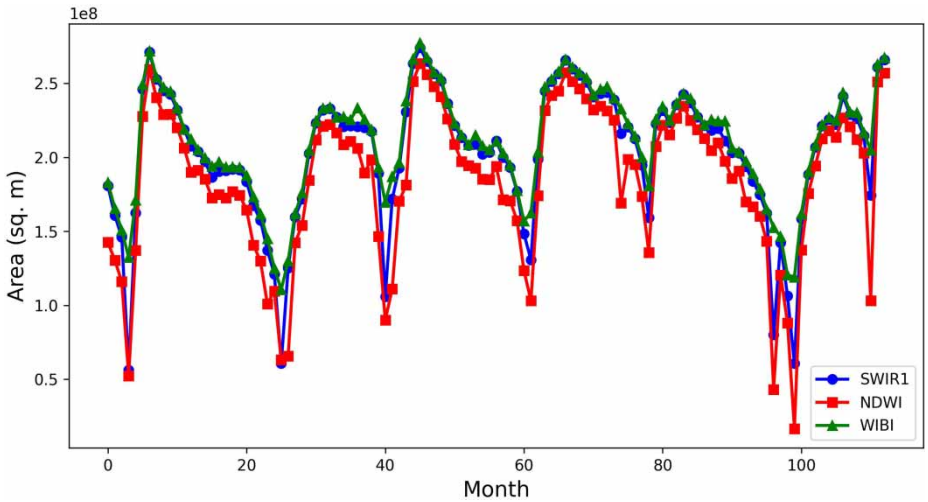

Figure 8 | Plots showing index-wise area variation trends of Manchar Lake as obtained from satellite images, using the three methods, SWIR1, NDWI (Green, NIR) and WIBI, taken at three different times of the year (M1, M2 and M3) for seven consecutive years (2013–2019). M1, M2 and M3, respectively, refer to the three selected months of January, May and September.

rest of the country received the usual normal rain. The rainfall was moderately above normal for the whole country in the month of September, whereas in Sindh recorded rainfall was close to normal.

In 2016, right after the end of the monsoon season, the country received 25% increase in rainfall during August, which was restored to normal in September. Before this monsoon, in July, the country experienced relatively scarce rainfall in which eastern parts of Sindh suffered a lot with almost no rainfall during the whole month.

In July 2017, Sindh was in a better position, close to normal, as compared to the rest of the country where the amount of rain was below normal. The situation continued over the country during the months of August and September. This time, the only exceptions were the regions of Punjab and Gilgit-Baltistan receiving close to normal and above normal rains respectively.

In 2018, below normal rainfall was recorded in the monsoon season. During September, country rainfall was below normal and below normal rainfall was observed in Sindh too. In August, both country and regional rainfall was below normal. In July, country rainfall was below normal and was below normal all over Sindh.

During the monsoon (July–September) season 2019, close to normal rainfall was recorded in the whole country. The seasonal rainfall was above normal over Sindh. In the September 2019, slightly above normal rainfall was recorded over the country. On the provincial scale, above normal rainfall was observed. In August 2019, close to normal rainfall was recorded over the country and above normal rainfall was observed in Sindh. On the provincial scale, during the month of July 2019, above normal rainfall was recorded over Sindh (Pakistan Meteorological Department).

CONCLUSIONS

Satellite imagery data containing the maps of water resources can be subjected to various water indices and can be effectively used in the management of the corresponding water resource. This research work analyzed various contemporary water detection bands and indices for their capabilities, selecting three of them, namely SWIR1, NDWI and WIBI, of which the WIBI is a novel one specifically derived as part of this research work. The main aim of the study was to develop remote-sensing and monitoring methods for water resources in Pakistan, where officially much less information is available on the existing significant water bodies. The selected indices were applied to the Landsat-8 OLI imagery to delineate a very significant lake, the Manchar Lake in the Sindh Province of Pakistan, calculating lake area over a period of 7 years. As exact *in situ* measurements were not available for the water body under study, the introduced index WIBI was calibrated over a man-made pool with a fixed and regular surface area. The results for Manchar Lake were validated qualitatively against the annual meteorological reports generated by the Climate Data Centre of Pakistan Meteorological Department as well as statistically against minimum area recorded for the water body as reported by the available resources, to show that WIBI performed best among all giving the most clear water body detection, proving it to be a better index for natural boundaries including muddy fields and trees. The theoretical basis of WIBI was intuitively derived; however, the validity of the proposed can be further investigated by comparing the results with other existing modified indices. Also, the proposed study can be extended by assessing new water indices and running the processes for every month rather than just three times a year. Sophisticated algorithms can also be devised to automate the process. Moreover, statistical and thematic accuracies of the detected water body images can be tested by comparing with *in situ* measurement area and the corresponding high-resolution images, respectively. For an agricultural country like Pakistan, such analysis can improve the monitoring and preservation of natural resources, especially water bodies, and hence can play a key role in the development of the country. With increasing volumes of available satellite data and GEE's powerful resource at hand, remote-sensing cloud computing platform is likely to be the central trend in such projects in future.

DATA AVAILABILITY STATEMENT

All relevant data are available from an online repository or repositories. USGS Landsat 8 Collection 1 Tier 1 TOA Reflectance https://developers.google.com/earth-engine/datasets/catalog/LANDSAT_LC08_C01_T1_TOA

REFERENCES

Acharya, T. D., Subedi, A., Yang, I. T. & Lee, D. H. 2017 Combining water indices for water and background threshold in Landsat image. *Multidisciplinary Digital Publishing Institute Proceedings* **2** (3), 143. https://doi.org/10.3390/ecsa-4-04902

Acharya, T. D., Subedi, A. & Lee, D. H. 2018 Evaluation of water indices for surface water extraction in a Landsat 8 scene of Nepal. *Sensors* **18**, 2580.

Acharya, T. D., Subedi, A. & Lee, D. H. 2019 Evaluation of machine learning algorithms for surface water extraction in a Landsat 8 scene of Nepal. *Sensors* **19**, 2769.

Campos, J. C. & Brito, J. C. 2018 Mapping underrepresented land cover heterogeneity in arid regions: the Sahara-Sahel example. *ISPRS Journal of Photogrammetry and Remote Sensing* **146**, 211–220.

El-Asmar, H. M., Hereher, M. E. & El Kafrawy, S. B. 2013 Surface area change detection of the Burullus Lagoon, North of the Nile Delta, Egypt, using water indices: a remote sensing approach. *The Egyptian Journal of Remote Sensing and Space Science* **16**, 119–123.

Feyisa, G. L., Meilby, H., Fensholt, R. & Proud, S. R. 2014 Automated water extraction index: a new technique for surface water mapping using Landsat imagery. *Remote Sensing of Environment* **140**, 23–35.

Gautam, V. K., Gaurav, P. K., Murugan, P. & Annadurai, M. 2015 Assessment of surface water dynamics in Bangalore using WRI, NDWI, MNDWI, supervised classification and K-T transformation. *Aquatic Procedia* **4**, 739–746. https://doi.org/10.1016/j.aqpro.2015.02.095.

Gorelick, N., Hancher, M., Dixon, M., Ilyushchenko, S., Thau, D. & Moore, R. 2017 Google earth engine: planetary-scale geospatial analysis for everyone. *Remote Sensing of Environment* **202**, 18–27.

Hansen, M. C., Potapov, P. V., Moore, R., Hancher, M., Turubanova, S. A., Tyukavina, A., Thau, D., Stehman, S., Goetz, S. J., Loveland, T. R., Kommareddy, A., Egorovl, A., Chini, L., Justice, C. O. & Townshend, J. R. G. 2013 High-resolution global maps of 21st-century forest cover change. *Science* **342**, 850–853.

Huang, X., Xie, C., Fang, X. & Zhang, L. 2015 Combining pixel-and object-based machine learning for identification of water-body types from urban high-resolution remote-sensing imagery. *IEEE Journal of Selected Topics in Applied Earth Observations and Remote Sensing* **8**, 2097–2110.

Huang, C., Chen, Y., Zhang, S. & Wu, J. 2018 Detecting, extracting, and monitoring surface water from space using optical sensors: a review. *Reviews of Geophysics* **56**, 333–360.

Hui, F., Xu, B., Huang, H., Yu, Q. & Gong, P. 2008 Modelling spatial-temporal change of Poyang Lake using multitemporal Landsat imagery. *International Journal of Remote Sensing* **29**, 5767–5784.

Ji, L., Zhang, L. & Wylie, B. 2009 Analysis of dynamic thresholds for the normalized difference water index. *Photogrammetric Engineering and Remote Sensing* **75**, 1307–1317.

Jiang, W., He, G., Long, T., Ni, Y., Liu, H., Peng, Y., Lv, K. & Wang, G. 2018 Multilayer perceptron neural network for surface water extraction in Landsat 8 OLI satellite images. *Remote Sensing* **10**, 755.

Kshetri, T. 2018 *NDVI, NDBI & NDWI Calculation Using Landsat 7, 8*. Available from: https://www.researchgate.net/publication/327971920_NDVI_NDBI_NDWI_Calculation_Using_Landsat_7_8.

Li, W., Du, Z., Ling, F., Zhou, D., Wang, H., Gui, Y., Sun, B. & Zhang, X. 2013 A comparison of land surface water mapping using the normalized difference water index from TM, ETM+ and ALI. *Remote Sensing* **5**, 5530–5549.

Li, L., Su, H., Du, Q. & Wu, T. 2021 A novel surface water index using local background information for long term and large-scale Landsat images. *ISPRS Journal of Photogrammetry and Remote Sensing* **172**, 59–78.

Malthus, T. & Dekker, A. 1995 First derivative indices for the remote sensing of inland water quality using high spectral resolution reflectance. *Environment International* **21**, 221–232.

Markert, K. N., Markert, A. M., Mayer, T., Nauman, C., Haag, A., Poortinga, A., Bhandari, B., Thwal, N. S., Kunlamai, T., Chishtie, F., Kwant, M., Phongsapan, K., Clinton, N., Towashiraporn, P. & Saah, D. 2020 Comparing sentinel-1 surface water mapping algorithms and radiometric terrain correction processing in Southeast Asia utilizing Google Earth Engine. *Remote Sensing* **12**, 2469.

McFeeters, S. K. 1996 The use of the normalized difference water index (NDWI) in the delineation of open water features. *International Journal of Remote Sensing* **17**, 1425–1432.

Muzaffer, R., Zaidi, A. Z. & ul Haque, S. 2020 Water balance study of Manchar Lake (Sindh, Pakistan) using Landsat and Sentinel 3A. In: *IGARSS 2020 – 2020 IEEE International Geoscience and Remote Sensing Symposium*. IEEE, Waikoloa, HI, USA, pp. 4770–4773. https://doi.org/10.1109/IGARSS39084.2020.9324492.

Pakistan Meteorological Department n.d. Available from: https://www.pmd.gov.pk.

Panoramas.cz n.d. 360globe.net. Available from: https://www.360globe.net/czech-republic/ostrava/open-air-swimming-pool.

Pekel, J.-F., Cottam, A., Gorelick, N. & Belward, A. S. 2016 High-resolution mapping of global surface water and its long-term changes. *Nature* **540**, 418–422.

Pickens, A. H., Hansen, M. C., Hancher, M., Stehman, S. V., Tyukavina, A., Potapov, P., Marroquin, B. & Sherani, Z. 2020 Mapping and sampling to characterize global inland water dynamics from 1999 to 2018 with full Landsat time-series. *Remote Sensing of Environment* **243**, 111792.

Rokni, K., Ahmad, A., Selamat, A. & Hazini, S. 2014 Water feature extraction and change detection using multitemporal Landsat imagery. *Remote Sensing* **6**, 4173–4189.

Sakamoto, T., Van Nguyen, N., Kotera, A., Ohno, H., Ishitsuka, N. & Yokozawa, M. 2007 Detecting temporal changes in the extent of annual flooding within the Cambodia and the Vietnamese Mekong Delta from MODIS time-series imagery. *Remote Sensing of Environment* **109**, 295–313.

Sarp, G. & Ozcelik, M. 2017 Water body extraction and change detection using time series: a case study of Lake Burdur, Turkey. *Journal of Taibah University of Science* **11**, 381–391.

Schaffer-Smith, D., Swenson, J. J., Barbaree, B. & Reiter, M. E. 2017 Three decades of Landsat-derived spring surface water dynamics in an agricultural wetland mosaic; implications for migratory shorebirds. *Remote Sensing of Environment* **193**, 180–192.

Song, C., Huang, B., Ke, L. & Richards, K. S. 2014 Remote sensing of alpine lake water environment changes on the Tibetan Plateau and surroundings: a review. *ISPRS Journal of Photogrammetry and Remote Sensing* **92**, 26–37.

Sun, F., Sun, W., Chen, J. & Gong, P. 2012 Comparison and improvement of methods for identifying waterbodies in remotely sensed imagery. *International Journal of Remote Sensing* **33**, 6854–6875.

Sun, W., Du, B. & Xiong, S. 2017 Quantifying sub-pixel surface water coverage in urban environments using low-albedo fraction from Landsat imagery. *Remote Sensing* **9**, 428.

USGS.gov. Science for a changing world. Available from: https://www.usgs.gov/special-topic/science-a-changing-world.

Wagle, N., Acharya, T. D., Kolluru, V., Huang, H. & Lee, D. H. 2020 Multi-temporal land cover change mapping using Google Earth Engine and ensemble learning methods. *Applied Sciences* **10**, 8083.

Wang, C., Jia, M., Chen, N. & Wang, W. 2018 Long-term surface water dynamics analysis based on Landsat imagery and the Google Earth Engine platform: a case study in the middle Yangtze River Basin. *Remote Sensing* **10**, 1635.

Wu, W., Shen, X., Zou, L., Lu, S. & Zhang, G. 2008 An integrated method for water body detection and delineation using Landsat ETM+ data. *Bulletin of Science Technology* **24**, 252–259.

Wu, Q., Lane, C. R., Li, X., Zhao, K., Zhou, Y., Clinton, N., DeVries, B., Golden, H. E. & Lang, M. W. 2019 Integrating LiDAR data and multi-temporal aerial imagery to map wetland inundation dynamics using Google Earth Engine. *Remote Sensing of Environment* **228**, 1–13.

Xu, H. 2006 Modification of normalised difference water index (NDWI) to enhance open water features in remotely sensed imagery. *International Journal of Remote Sensing* **27**, 3025–3033.

Yang, X., Zhao, S., Qin, X., Zhao, N. & Liang, L. 2017 Mapping of urban surface water bodies from Sentinel-2 MSI imagery at 10 m resolution via NDWI-based image sharpening. *Remote Sensing* **9**, 596.

First received 18 July 2021; accepted in revised form 7 November 2021. Available online 24 November 2021